ACS Photonics

Article

pubs.acs.org/journal/apchd5

Angular-Momentum-Biased Nanorings To Realize Magnetic-Free Integrated Optical Isolation

Dimitrios L. Sounas and Andrea Alù*

Department of Electrical and Computer Engineering, The University of Texas at Austin, Austin, Texas 78712, United States

Supporting Information

ABSTRACT: We present the concept and practical design of nonreciprocal optical nanodevices that do not require magnetic materials or bias, but instead are based on a fully integrated nanophotonic ring resonator spatiotemporally modulated to impart angular momentum bias that, according to the Onsager−Casimir principle, can break time-reversal symmetry. On the basis of this idea, we discuss optimal designs for compact optical isolators exhibiting arbitrarily large isolation and low transmission loss, achieved by properly selecting the quality factor of the nanoring, the amount of angular momentum bias, and the gaps between ring and channel/drop waveguides. A practical implementation based on stepwise modulation and pin junctions is explored, showing strong nonreciprocal response in a simple, integrated design. These findings can enable the realization of on-chip, fully integrable nonreciprocal optical nanocomponents as a new paradigm in all-optical communication systems.

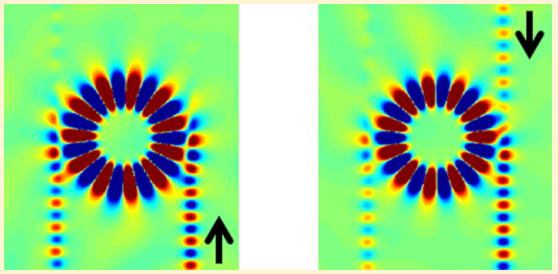

KEYWORDS: *nonreciprocity, spatiotemporal modulation, optical isolator, optical circulator, optical nanodevices*

The symmetry in wave transmission between two points in space is a direct consequence of time-reversal symmetry,[1] and, as such, it is a fundamental property in many physical problems, including electromagnetic,[2] acoustic,[3] and thermodynamic[4] systems. In many practical instances this reciprocal response needs to be broken, such as when a source has to be isolated from the load or when a receiver and a transmitter are connected to the same transmission channel, with their interference being obviously unwanted. This need has become particularly important in nanophotonics, due to the large interest in realizing all-optical on-chip communication systems.

Nonreciprocal transmission in a linear system requires biasing the system with a vector whose direction is reversed under time reversal,[1] like the magnetic field vector. To date, nonreciprocity in optics has been indeed almost exclusively obtained using magneto-optic effects, arising in certain magnetic media, such as ferrites, when biased by a static magnetic field.[5] However, the lattice mismatch between ferrites and semiconductors makes the integration of magneto-optical components in nanophotonic systems very problematic.[6] Furthermore, the weak nature of the magneto-optic effect in optics results in very bulky devices, several orders of magnitude larger than the wavelength.[7,8] Resonances have been successfully exploited to reduce the device footprint, but relevant designs are still difficult to integrate.[9−11] Although a method for integration of magneto-optic and semiconducting materials has been recently proposed in ref 12, the drawbacks related to the requirement of a static magnetic bias still hold. Plasmonic structures, which are in principle integrable, can enhance magneto-optical activity,[13−15] however at the expense of higher loss and without avoiding the need of an external bias.

The issues associated with magneto-optics have spurred significant interest in obtaining magnetic-free nonreciprocal response. Nonlinearities can break time-reversal symmetry,[16−20] but the operation of the resulting devices strongly depends on the input field intensity, thus making them unsuitable for applications involving small signals, as in quantum information processing. Furthermore, nonlinearities result in spurious harmonics that are usually undesirable. Linear nonreciprocity can be achieved in spatiotemporally modulated waveguides by appropriate electric[6,21−24] or acoustic[25] bias. Although the bandwidth of such devices can be large, their electrical size is usually significantly larger than the wavelength, due to the weak nature of electro- and acousto-optic effects. Opto-mechanical resonators can also exhibit linear nonreciprocity,[26,27] however usually over a narrow bandwidth, again due to the weak nature of opto-mechanical effects. Nonreciprocity has also been demonstrated in transistor-loaded metamaterials,[28,29] but these approaches are limited to subterahertz waves where transistors are available.

Recently, a concept to produce large linear nonreciprocity for electromagnetic waves at the subwavelength scale by biasing with the angular-momentum vector has been theoretically introduced in ref 30 based on a suitable form of spatiotemporal modulation imparted by circulating signals. Here we show how this general concept can be successfully employed to introduce a new paradigm for nonreciprocal nanophotonic devices, realizing magnetic-free, fully integrable, compact optical isolators based on channel-drop filters with spatiotemporally

Received: September 30, 2013
Published: January 17, 2014

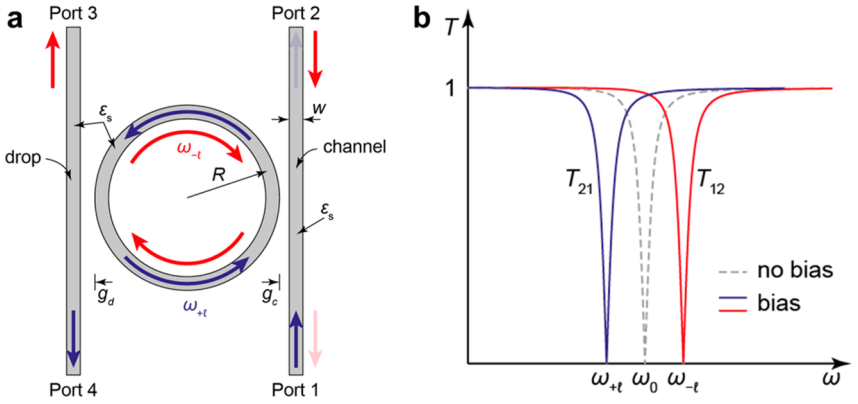

Figure 1. Optical isolator based on channel-drop filter. (a) Channel-drop filter consisting of a microring resonator between two parallel waveguides. The ring supports pairs of right- and left-handed modes, excited by incident waves from ports 1 and 2, respectively. At the right-handed resonance ω_{+l} power entering from port 1 couples to port 4, creating a transmission zero at port 2, while at the left-handed resonance ω_{-l} power entering from port 2 couples to port 3, creating a transmission zero at port 1. (b) Transmission between ports 1 and 2. In a conventional ring (gray dashed line), $\omega_{+l} = \omega_{-l} = \omega_l$ and the structure is reciprocal ($T_{21} = T_{12}$). Application of an appropriate bias (solid lines) can remove the degeneracy between the modes of opposite handedness and create nonreciprocity ($T_{21} \neq T_{12}$). At ω_{+l} and ω_{-l} waves can propagate only from port 2 to 1 and from port 1 to 2, respectively.

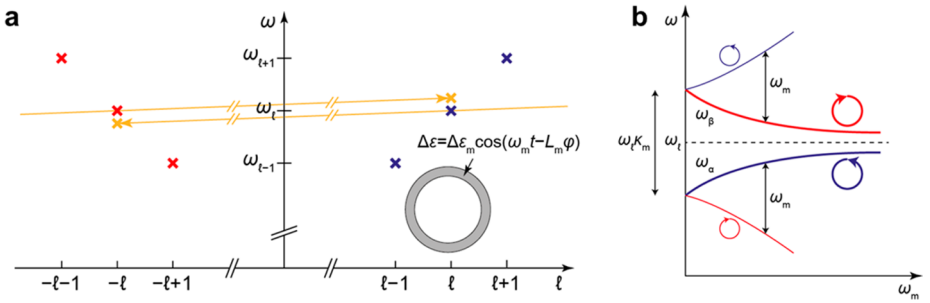

Figure 2. Angular-momentum-induced nonreciprocity. (a) Effect of a spatiotemporal permittivity modulation $\Delta\varepsilon = \Delta\varepsilon_m \cos(\omega_m t - L_m\varphi)$ on the states of a ring resonator. The modulation generates the nonresonant states $|l - L_m, \omega_l - \omega_m\rangle$ and $|-l + L_m, \omega_l + \omega_m\rangle$ (orange crosses) out of the resonant ones $|l, \omega_l\rangle$ and $|-l, \omega_l\rangle$, respectively. For $L_m = 2l$ and $\omega_m \ll \omega_l$, $|l - L_m, \omega_l - \omega_m\rangle$ and $|-l + L_m, \omega_l + \omega_m\rangle$ resonantly couple to $|-l, \omega_l\rangle$ and $|+l, \omega_l\rangle$, giving rise to the hybrid states of panel b. (b) Frequency diagram of the ring states after a dynamic modulation with frequency $\omega_m \neq 0$ is applied. The $|\alpha\rangle$ and $|\beta\rangle$ states of the modulated ring are hybridizations of the $|\pm l\rangle$ states. The substates have different strengths and lie at frequency levels separated by ω_m, hence producing nonreciprocity.

modulated rings as their core element. Temporal coupled mode theory (CMT) is used to analytically model the proposed nanostructures, showing excellent agreement with finite-difference time-domain (FDTD) full-wave simulations. Our model determines the optimal conditions for maximum isolation and minimum transmission loss in terms of the available quality (Q-) factor of the nanoring resonator and its coupling to feeding monomodal waveguides. A simplified implementation of the proposed nanoisolator by means of a stepwise modulation profile, which may be readily implemented via carrier injection/depletion in silicon (Si) pin junctions, is also presented, in addition to a comparison with a recently proposed solution for magnetless nonreciprocity, based on a different type of spatiotemporal modulation.

RESULTS AND DISCUSSION

Consider the channel-drop filter of Figure 1a, consisting of a ring resonator placed between two parallel waveguides. The nanoring supports pairs of degenerate counter-propagating states with azimuthal dependences $e^{\pm il\varphi}$, where l is an integer. The lth pair resonates when the circumference of the ring is l times the guided wavelength. Right- and left-handed states may be excited by incident waves from ports 1 and 2, respectively, due to the forward nature of the coupling between the waveguides and the ring. When the excitation frequency coincides with the ring resonance, a transmission dip occurs between the ports of the channel waveguide. If $\tau = \tau_c/2$, where τ is the total relaxation time of the ring, including thermal loss, radiation loss, and coupling to the waveguides, and τ_c is the relaxation time due to coupling to the channel waveguide, the transmission dip between ports 1 and 2 is identically zero.[31]

Let us assume now that we can remove the degeneracy between the $|\pm l\rangle$ states, so that $|+l\rangle$ and $|-l\rangle$ resonate at different frequencies ω_{+l} and ω_{-l}, respectively ($\omega_{+l} < \omega_{+l}$ in Figure 1b). Then, $T_{21} = 0$ and $T_{12} = 0$ at ω_{+l} and ω_{-l}, respectively, where T_{ij} is the transmission coefficient from port j to i. Selecting $\Delta\omega = \omega_{-l} - \omega_{+l} > \mathrm{BW}_{-l}$, where BW_{-l} is the bandwidth of the $|-l\rangle$ resonance, $T_{21} = 0$ and $T_{12} \approx 1$ at ω_{+l}, thus realizing an almost perfect isolator from port 1 to 2, in principle with infinite isolation, $\mathrm{IS} = 20\log_{10}(T_{12}/T_{21}) \to \infty$, and negligible transmission loss. Similarly, if $\Delta\omega > \mathrm{BW}_{+l}$, $T_{21} \approx 1$ and $T_{12} = 0$ at ω_{-l}, realizing an almost perfect isolator from port 2 to 1. For $\Delta\omega \ll \omega_l$ the resonance bandwidth is not affected by the lift of degeneracy, so that $\mathrm{BW}_{+l} = \mathrm{BW}_{-l} = \mathrm{BW}_l$, where $\mathrm{BW}_l = \omega_l/Q_l$ is the resonance bandwidth of the

dx.doi.org/10.1021/ph400058y | ACS Photonics 2014, 1, 198−204

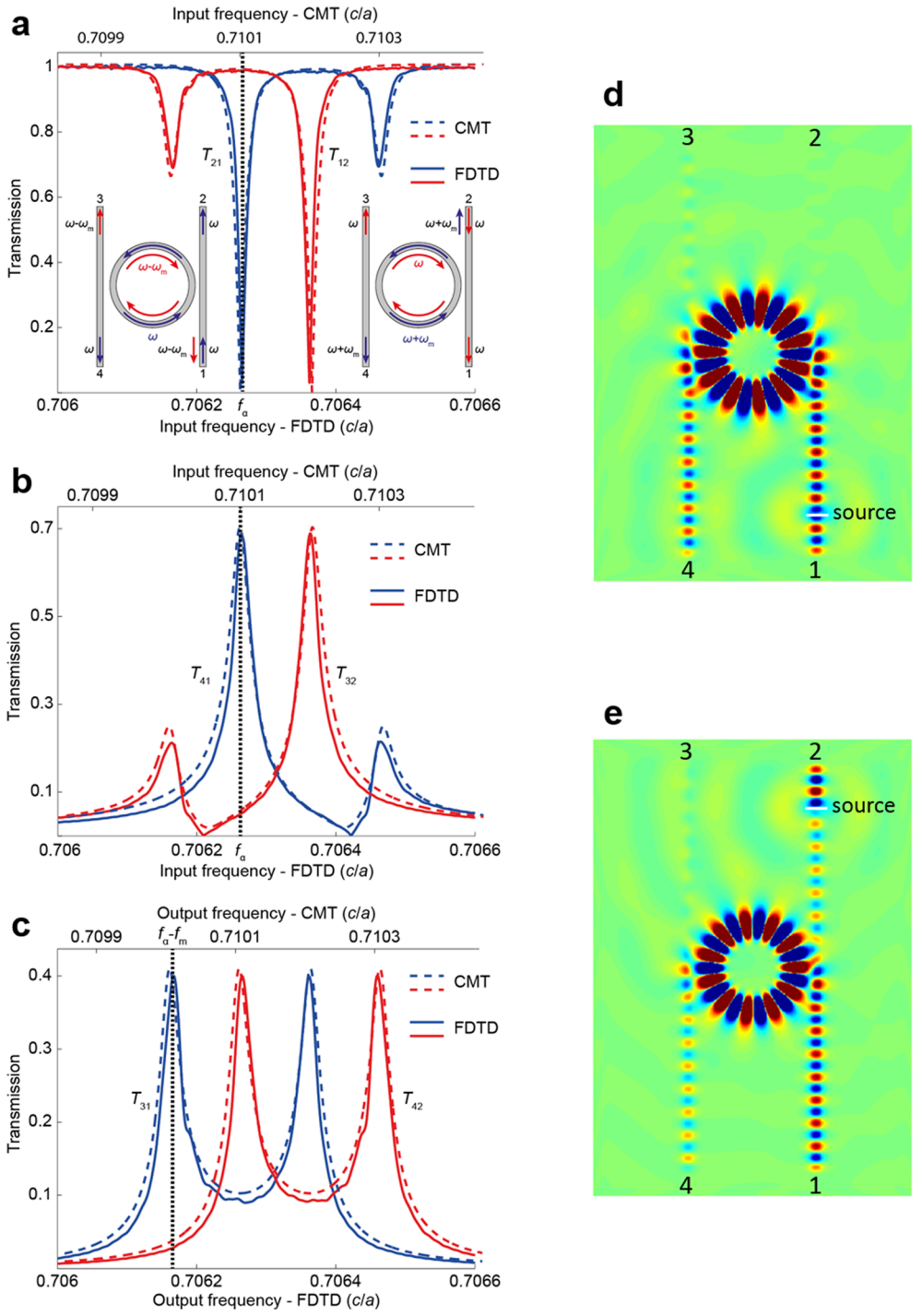

Figure 3. Transmission properties of a spatiotemporally modulated channel-drop filter. An ideal permittivity modulation in the form $\Delta\varepsilon = \Delta\varepsilon_m \cos(\omega_m t - L_m\varphi)$ is assumed. (a) Transmission between ports 1 and 2 as a function of the input frequency. Here the output frequency coincides with the input frequency. An incident wave of frequency ω from port 1 (left inset) excites the right-handed substates at frequency ω, which subsequently leak to ports 2 and 4. Due to the hybrid nature of the ring states, the left-handed substates are also excited at frequency $\omega - \omega_m$ and subsequently leak to ports 1 and 3. On the contrary, an incident wave of frequency ω from port 2 (right inset) excites the left-handed substates at frequency ω, which leak to ports 1 and 3, and the right-handed substates at frequency $\omega + \omega_m$, which leak to ports 2 and 4. (b) Transmission from port 1 to 4 and from port 2 to 3 versus the input frequency, which, like in panel a, coincides with the output frequency here. (c) Transmission from port 1 to 3 and from port 2 to 4 versus output frequency at these ports. Contrary to panels a and b, the output frequency is now red-/blue-shifted by the quantity ω_m with respect to the input frequency for excitation from ports 1 and 2, respectively. (d) Field profile at f_α (dotted line in panels a, b, and c) for excitation from port 1. (e) The same as in panel d, but for excitation from port 2. The results in panels a−c were derived via CMT and FDTD simulations. The results in panels d and e were derived via FDTD simulations. They all take into account of intermodulation products and frequency mixing, as described above. The parameters of the structure are $w = 0.2a$, $R = 0.88a$, $g_1 = 0.3a$, $g_2 = 0.33a$, $\Delta\varepsilon_m = 5 \times 10^{-4}\varepsilon_s$, $\varepsilon_s = 12$, $f_m = 10^{-4}c/a$, and $L_m = 22$, where a is an arbitrary reference length.

dx.doi.org/10.1021/ph400058y | ACS Photonics 2014, 1, 198−204

degenerate modes and Q_l is the corresponding Q-factor. Then, $\Delta\omega > \mathrm{BW}_l$ becomes

$$\frac{\Delta\omega}{\omega_l} Q_l > 1 \tag{1}$$

which is the condition for obtaining maximum isolation with minimum transmission loss.

The conventional way of removing the degeneracy between $|\pm l\rangle$ states is by loading the nanoring with a magneto-optical material, inducing different guided wavelengths for opposite propagation directions. However, as already mentioned, magneto-optical devices are difficult to integrate in nanophotonic systems because they involve bulky biasing magnets and materials that are incompatible with semiconductor technology. In ref 30 it was shown that an alternative way to achieve a similar degeneracy lift is to apply an azimuthal spatiotemporal modulation $\Delta\varepsilon = \Delta\varepsilon_\mathrm{m} \cos(\omega_\mathrm{m} t - L_\mathrm{m}\varphi)$ to the material loading the nanoring, as illustrated in the inset of Figure 2a. As discussed later, such an approach can be fully implemented in Si-based technology, and, therefore, it is totally compatible with modern integrated nanophotonic systems.

In ref 30 it was also shown that the optimal way to remove the degeneracy between the $|\pm 1\rangle$ states is by choosing $L_\mathrm{m} = 2$ and ω_m small but nonzero, so that $|\pm 1\rangle$ resonantly couple to each other and two new hybrid states are created, each of which is a superposition of the $|\pm 1\rangle$ states, however now with different frequencies. Here, we apply this result to an arbitrary pair of states $|\pm l\rangle$ by selecting $L_\mathrm{m} = 2l$, so that $|\pm l\rangle$ resonantly couple to each other, as illustrated in Figure 2a, and the hybrid states $|\alpha\rangle$ and $|\beta\rangle$, depicted in Figure 2b, are generated. This generalization is especially important for the problem at hand, because of the necessity to excite a sufficiently large resonance Q-factor in the nanoring to minimize the requirements on modulation amplitude, as discussed in the following. Both $|\alpha\rangle$ and $|\beta\rangle$ consist of dominant and secondary substates of opposite handedness and frequencies separated by ω_m. The dominant substates of $|\alpha\rangle$ and $|\beta\rangle$ are $|+l\rangle$ and $|-l\rangle$ with frequencies $\omega_\alpha = \omega_l - \delta\omega/2$ and $\omega_\beta = \omega_l + \delta\omega/2$, respectively, where $\delta\omega = \sqrt{\omega_\mathrm{m}^2 + \omega_l^2\kappa_\mathrm{m}^2} - \omega_\mathrm{m}$ and κ_m is the coupling coefficient as given by eq 2 of ref 30. The maximum separation between any two substates of opposite handedness, which determines the strength of nonreciprocity, is shown in ref 30 to be $\Delta\omega = \omega_l\kappa_\mathrm{m}/\sqrt{3}$ and it occurs for $\omega_\mathrm{m} = \omega_l\kappa_\mathrm{m}/\sqrt{3}$. Then, eq 1 becomes

$$\kappa_\mathrm{m} Q_l \geq \sqrt{3} \tag{2}$$

which, for a given κ_m, i.e., for a given $\Delta\varepsilon_\mathrm{m}$, determines the minimum required Q-factor for observing strong nonreciprocity with low transmission loss.

A particularly interesting case is the transmission between the different ports of the proposed channel waveguide. Transmission from port 1 to 2 is given by (see the Supporting Information for details)

$$T_{21} = \frac{(\omega - \omega_l + i\tau^{-1} - i2\tau_\mathrm{c}^{-1})(\omega - \omega_\mathrm{m} - \omega_l + i\tau^{-1}) - \omega_l^2\kappa_\mathrm{m}^2/4}{(\omega - \omega_l + i\tau^{-1})(\omega - \omega_\mathrm{m} - \omega_l + i\tau^{-1}) - \omega_l^2\kappa_\mathrm{m}^2/4} \tag{3}$$

and becomes zero when its numerator is zero, leading to

$$\begin{aligned}(\omega - \omega_l)(\omega - \omega_\mathrm{m} - \omega_l) - \tau^{-1}(\tau^{-1} - 2\tau_\mathrm{c}^{-1}) - \omega_l^2\kappa_\mathrm{m}^2 &= 0\\ \tau^{-1}(\omega - \omega_l) + (\tau^{-1} - 2\tau_\mathrm{c}^{-1})(\omega - \omega_\mathrm{m} - \omega_l) &= 0\end{aligned} \tag{4}$$

For high-Q resonances, as the case of interest here to keep the requirement of modulation frequency and amplitude low, the relaxation time is much larger than the resonance period $\omega_l\tau \gg 1$, and the first of eqs 4 is satisfied by $\omega = \omega_\alpha$ or $\omega = \omega_\beta + \omega_\mathrm{m}$. However, only $\omega = \omega_\alpha$ can also satisfy the second of eqs 4, leading to

$$\tau_\mathrm{d} = \tau_\mathrm{c}\left(1 + \frac{\delta\omega}{\omega_\mathrm{m}}\right) \tag{5}$$

where τ_d is the relaxation time due to coupling to the drop waveguide. This equation is derived under the assumption that thermal and radiation losses are negligible compared to loss due to coupling to the channel/drop waveguides, a valid assumption for high-order modes, leading to $\tau^{-1} = \tau_\mathrm{c}^{-1} + \tau_\mathrm{d}^{-1}$. Equation 5 is the condition for $T_{21} = 0$ at ω_α and hence infinite isolation from port 1 to 2. Following a similar analysis for T_{12}, it may be shown that eq 5 is also the condition for $T_{12} = 0$ at ω_β and hence infinite isolation from port 2 to 1. We note that the temporal modulation inherently introduces additional frequencies into the picture, which are fully taken into account in our analysis. As sketched in the inset of Figure 3, the intermodulation frequencies are routed towards specific ports, as detailed in the caption of Figure 3 and below.

The material with the strongest known permittivity modulation to date for nanophotonic applications is silicon, with $\Delta\varepsilon_\mathrm{m} = 5 \times 10^{-4}\varepsilon_\mathrm{s}$, where $\varepsilon_\mathrm{s} = 12$ is its permittivity.[6,32,33] This value leads to $\kappa_\mathrm{m} = 2.5 \times 10^{-4}$ and a required $Q_l \geq 7000$, according to eq 2. For a ring resonator with $w = 0.2a$ and $R = 0.88a$, where a is an arbitrary reference length, such a Q-factor can be achieved with $l = 11$ and a minimum gap between the nanoring and the waveguides of $0.3a$. Selecting $g_\mathrm{c} = 0.3a$, g_d should be equal to $0.33a$ so that eq 5 is satisfied for $\Delta\omega = \omega_\mathrm{m}$, i.e., for the case of maximum separation between any two states of opposite handedness.

Transmission between the ports of the proposed modulated channel-drop filter was calculated via CMT and FDTD full-wave simulations and is presented in Figure 3a–c. The agreement between CMT and FDTD simulations is excellent, apart from a slight frequency shift, attributed to the inherent dispersion of the FDTD method.[31] In perfect agreement with our design, $T_{21} \approx 0$ and $T_{12} \approx 1$ at $f_\alpha = \omega_\alpha/(2\pi)$ (Figure 3a), corresponding to an isolation from port 1 to 2 of more than 35 dB and a transmission loss of less than 1 dB. Similarly, $T_{12} \approx 0$ and $T_{21} \approx 1$ at $f_\beta = \omega_\beta/(2\pi)$, indicating an isolation from port 2 to 1 with the same properties as from port 1 to 2. Smaller transmission dips for T_{21} and T_{12} also exist at $f_\beta + f_\mathrm{m}$ and $f_\alpha - f_\mathrm{m}$, respectively, due to coupling to the secondary $|+l\rangle$ and $|-l\rangle$ substates of $|\alpha\rangle$ and $|\beta\rangle$. As explained above, secondary substates do not satisfy eq 5 and therefore cannot yield transmission zeros. We reiterate that in this panel input and output frequencies are the same, i.e., we do not observe intermodulation products in the transmission from port 1 to 2, or vice versa.

Apart from transmission between the ports of the channel waveguide, it is also interesting to explore what happens to the ports of the drop waveguide. The $|+l\rangle$ substates leak to ports 2 and 4, while the $|-l\rangle$ substates leak to ports 1 and 3. For

dx.doi.org/10.1021/ph400058y | ACS Photonics 2014, 1, 198–204

excitation from port 1 at frequency ω, the $|+l\rangle$ substates are directly excited by the incident field at frequency ω, while the $|-l\rangle$ substates are indirectly excited at the different frequency $\omega - \omega_m$. Therefore, the frequencies of the signals delivered to ports 3 and 4 are $\omega - \omega_m$ and ω, respectively, as illustrated in the left inset of Figure 3a. The maxima of the signal at port 4 (T_{41} curve of Figure 3b) occur at f_α and $f_\beta + f_m$, when the incident frequency coincides with the resonance frequency of the $|+l\rangle$ substates. The maxima of the signal at port 3 (T_{31} curve of Figure 3c) are red-shifted by f_m with respect to port 4, due to the same red-shift of the $|-l\rangle$ substate with respect to the $|+l\rangle$ one. Similar arguments also hold for excitation from port 2 and are graphically summarized in the insets of Figure 3a and in the T_{32} and T_{42} curves of Figure 3b and c, respectively. It is important to highlight that the output frequency in Figure 3c is shifted with respect to the input frequency by the quantity ω_m.

The device operation can be further understood by inspecting the electric field distribution plotted in Figure 3d and e at frequency f_α. For excitation from port 1 (Figure 3d), the power transmitted to port 2 is negligible, while most of the incident power is transmitted to port 4. Notice that not all of the incident power is transmitted to port 4 because a portion also couples to the $|-l\rangle$ substate of $|\alpha\rangle$ and therefore flows into port 3. However, this power is not visible in Figure 3d because it occurs at a different frequency ($f_\alpha - f_m$) from the one analyzed in Figure 3d. For excitation from port 2 (Figure 3e), almost all of the incident power reaches port 1, as expected. However, quite unexpectedly, a non-negligible amount of power seems to get reflected back to port 2 and transmitted to port 4. As mentioned above, outgoing signals at ports 2 and 4 are related to the $|+l\rangle$ substates, which cannot be excited at frequency f_α by an incident signal from port 2. The explanation for this peculiar behavior resides on the broadband pulse employed in the FDTD simulations, which excites the $|-l\rangle$ substate and subsequently the $|+l\rangle$ substate of the $|\alpha\rangle$ state at frequencies $f_\alpha - f_m$ and f_ω, respectively. Note that this issue would not arise in a practical design, because the bandwidth of transmitted signals will be smaller than the resonance bandwidth of the device, to avoid pulse distortion. The reason that such a pulse was not used in simulations is that it is several orders longer than the carrier signal period, and, as a result, it would lead to prohibitively long simulation times.

As explained before and illustrated in the insets of Figure 3a, excitation from ports 1 and 2 with frequency ω results in reflected signals with frequencies $\omega - \omega_m$ and $\omega + \omega_m$, respectively. It follows that for excitation of the structure with a pulse of bandwidth BW_s and center frequency ω, the corresponding reflected signals will also be pulses with the same bandwidth and center frequencies $\omega \pm \omega_m$. It is easy to see that in order for these modulation byproducts to not interfere with the original pulse, BW_s should be smaller than ω_m, which could make the reader think that the available bandwidth is limited by the modulation frequency. Nevertheless, under optimal operation, as described by eq 2, $\omega_m > BW_l$, and, since $BW_s < BW_l$ in order to avoid pulse distortion, the zero-overlap condition $\omega_m > BW_s$ is automatically satisfied. In other words, the bandwidth of a properly designed isolator is exclusively determined by the ring resonance and not by the modulation frequency.

The strongest electro-optical modulation to date in Si is achieved via carrier injection/depletion using suitably designed pin junctions.[32,33] In order to apply this technique to our nanophotonic design, the assumption of a continuous modulation needs to be approximated by a stepwise one, with different steps corresponding to different junctions. It may be a reasonable guess that at least four pin junctions per modulation period $2\pi/L_m$ are necessary to comply with Nyquist sampling criterion, resulting in $4L_m$ junctions for the entire ring (88 junctions in the $l = 11$ case), which is probably prohibitive to implement in practice. However, as we show next, this number may be drastically reduced to up to only three junctions. To this end, we assume that the continuous modulation profile is approximated with N steps:

$$\Delta\varepsilon = \Delta\varepsilon_m \sum_{n=0}^{N} \cos(\omega_m t - L_m\varphi_n)\ \mathrm{rect}\left(\frac{\varphi - \varphi_n}{\Delta\varphi}\right) \tag{6}$$

where rect(x) is a zero-centered rectangular pulse with width and height 1, $\Delta\varphi = 2\pi/N$ is the step width, and $\varphi_n = (n + 1/2)\Delta\varphi - \pi$ is the center of the nth step. Applying the Poisson summation formula to eq 6 (see Supporting Information for details) yields

$$\Delta\varepsilon = \Delta\varepsilon_m \sum_{k=-\infty}^{\infty} (-1)^{k(N-1)}\mathrm{sinc}\left(\frac{L_m + kN}{N}\right) \times \cos[\omega_m t - (L_m + kN)\varphi] \tag{7}$$

where $\mathrm{sinc}(x) = \sin(\pi x)/(\pi x)$. Equation 7 shows that the stepwise modulation of eq 6 is a superposition of an infinite number of continuous modulation profiles with different angular momenta. For $\omega_m \ll \omega_l$, only the one with $L_m + kN = 2l$ can resonantly couple the $|\pm l\rangle$ states and induce nonreciprocity. Then, the equivalent modulation amplitude is

$$\Delta\varepsilon_m^{eq} = \Delta\varepsilon_m\ \mathrm{sinc}\left(\frac{2l}{N}\right) \tag{8}$$

$\Delta\varepsilon_m^{eq}$ therefore decreases linearly with N, a reduction that can be easily compensated by the exponential increase of Q-factor with l or $g_{c,d}$. Attention should be paid to prevent $2l/N$ from coinciding with a zero of the sinc function. The minimum N for which this condition is met is indeed $N = 3$.

Consider first the extreme case $N = 3$: for $l = 11$, $\Delta\varepsilon_m^{eq} = 0.0376\Delta\varepsilon_m$, yielding $\kappa_m \approx 10^{-5}$, which requires a Q-factor around 200 000. Although Q-factors of this order have been reported in the literature in Si-based nanophotonic resonators,[34] they may be hard to achieve in practice. The required value of the Q-factor may be easily reduced by increasing N. For example, increasing N from 3 to 9 brings the required Q-factor from 200 000 down to 60 000. Further increasing N to 15 brings the Q-factor down to 35 000. Here, in order to show that the proposed discretization scheme works even in the extreme case $N = 3$, Figure 4 presents T_{21} and T_{12} for $N = 3$ and $\Delta\varepsilon_m = 5 \times 10^{-3}\varepsilon_s$, as calculated via both CMT and FDTD simulations. We used a larger value of $\Delta\varepsilon_m$ here to bring the required Q-factor down to 20 000, which allows keeping the simulation time to a reasonable level. Both analytical and simulated curves show that $T_{21} \approx 0$, $T_{12} \approx 1$ at frequency f_α and $T_{12} \approx 0$, $T_{21} \approx 1$ at f_β, as theoretically expected, demonstrating the efficiency of the proposed scheme.

Finally, we compare the proposed spatiotemporally modulated nanoring with the one theoretically discussed in the seminal paper[6] to realize magnetic-free optical isolation. First,

dx.doi.org/10.1021/ph400058y | ACS Photonics 2014, 1, 198−204

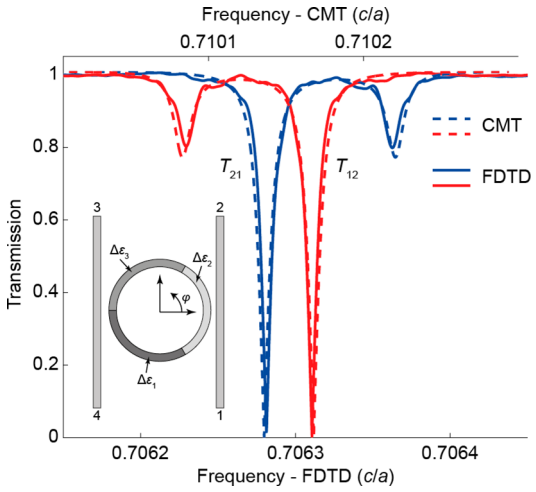

Figure 4. Transmission properties of a spatiotemporally modulated channel-drop filter with three distinct modulation regions along the ring. The permittivity modulation is $\Delta\varepsilon_1 = \Delta\varepsilon_m \cos(\omega_m t + 2\pi/3)$, $\Delta\varepsilon_2 = \Delta\varepsilon_m \cos(\omega_m t)$, and $\Delta\varepsilon_3 = \Delta\varepsilon_m \cos(\omega_m t - 2\pi/3)$ in the regions $-\pi < \varphi < -\pi/3$, $-\pi/3 < \varphi < \pi/3$, and $\pi/3 < \varphi < \pi$, respectively. Results are obtained via coupled-mode theory and FDTD simulations. The parameters of the structure are $w = 0.2a$, $R = 0.88a$, $g_1 = 0.33a$, $g_2 = 0.35a$, $\Delta\varepsilon_m = 5 \times 10^{-3}\varepsilon_s$, $\varepsilon_s = 12$, and $f_m = 5.3 \times 10^{-5}c/a$, where a is an arbitrary reference length.

we notice that the two functionalities are based on different principles: nonreciprocity in ref 6 is the result of an asymmetric mode conversion for opposite propagation directions in a multimodal waveguide. The fundamental mode supported by the nanoring is transformed into a higher-order mode for one propagation direction (left to right in Figure 3 of ref 6), while no conversion arises for the opposite direction (right to left in Figure 3 of ref 6). Since the fundamental and first higher-order modes are orthogonal across the waveguide cross-section, a *nonuniform modulation* profile is required for this conversion to happen. On the contrary, our approach is based on the lift of degeneracy of counter-propagating modes with identical cross-section profile, mimicking the case in which the ring was made of a magnetically biased material, a result that is achieved with an arguably easier-to-realize *uniform modulation* in the transverse cross-section. The proposed approach also allows minimizing the nanoring size and keeping the modulation requirements to a minimum, as dictated by eq 2. In addition, in the Supporting Information we prove that the proposed solution extends the operational bandwidth of the nonreciprocal response by over a factor of 4 compared to an analogous nanoring operated as proposed in ref 6.

CONCLUSIONS

A novel class of magnetic-free, fully integrable, nonreciprocal optical nanodevices relying on azimuthal spatiotemporal modulation of the nanoring resonator of a channel-drop filter has been introduced. Nonreciprocity follows from the removal of the degeneracy between states of opposite handedness in the modulated nanoring. By properly adjusting its resonance Q-factor and the coupling to the channel and drop waveguides, extremely high isolation with almost zero transmission loss can be achieved. Compact design rules have been rigorously derived for optimal designs, and a practical implementation by means of a stepwise modulation scheme implemented with pin junctions has been explored. The fact that angular-momentum biasing allows keeping the modulation frequency of the nanoring arbitrarily small significantly relaxes the minimum number of required pin junctions, up to only 3. It is remarkable that, in addition to realizing an isolator, the proposed structure can also operate as a quasi-ideal circulator, since incident power from ports 1, 2, and 4 is transmitted to ports 4, 1, and 3, respectively, while incident power from port 3 is mainly transmitted to port 2 with a small portion leaking to port 4 (since the zero-transmission condition is satisfied only from the side of the channel waveguide). We believe that the proposed concept may open exciting venues toward the full integration of nonreciprocal components such as isolators, circulators, and rotators in all-optical communication and nanophotonic systems.

ASSOCIATED CONTENT

Supporting Information

The Supporting Information includes coupled mode analysis for the spatiotemporally modulated channel-drop filter, the analysis of the stepwise modulation case, and a comparison of the bandwidth constraints between our proposed nonreciprocal operation and the one seminally introduced in ref 6. This material is available free of charge via the Internet at http://pubs.acs.org.

AUTHOR INFORMATION

Corresponding Author

*E-mail: alu@mail.utexas.edu.

Notes

The authors declare no competing financial interest.

ACKNOWLEDGMENTS

This work was partially supported by the DTRA YIP Award No. HDTRA1-12-1-0022 and the AFOSR YIP Award No. FA9550-11-1-0009.

REFERENCES

(1) Casimir, H. B. G. On Onsager's principle of microscopic reversibility. *Rev. Mod. Phys.* **1945**, *17*, 343−350.
(2) Harrington, R. F. *Time Harmonic Electromagnetic Fields*; John Wiley & Sons, 2001.
(3) Rayleigh, J. W. S. *The Theory of Sound Vol. II*; Macmillan & Co., 1896.
(4) Landau, L. D.; Lifshitz, E. M. *Statistical Physics, First Part*; Pergamon Press, 1968.
(5) Potton, R. J. Reciprocity in optics. *Rep. Prog. Phys.* **2004**, *67*, 717−754.
(6) Yu, Z.; Fan, S. Complete optical isolation created by indirect interband photonic transitions. *Nat. Photonics* **2009**, *3*, 91−94.
(7) Shintaku, T. Integrated optical isolator based on efficient nonreciprocal radiation mode conversion. *Appl. Phys. Lett.* **1998**, *73*, 1946−1948.
(8) Fujita, J.; Levy, M.; Osgood, R. M., Jr.; Wilkens, L.; Dötsch, H. Waveguide optical isolator based on Mach-Zehnder interferometer. *Appl. Phys. Lett.* **2000**, *76*, 2158−2160.
(9) Wang, Z.; Fan, S. Optical circulators in two-dimensional magneto-optical photonic crystals. *Opt. Lett.* **2005**, *30*, 1989−1991.
(10) Kono, N.; Kakihara, K.; Saitoh, K.; Koshiba, M. Nonreciprocal microresonators for the miniaturization of optical waveguide isolators. *Opt. Express* **2007**, *15*, 7737−7751.
(11) Jalas, D.; Petrov, A.; Krause, M.; Hampe, J.; Eich, M. Resonance splitting in gyrotropic ring resonators. *Opt. Lett.* **2010**, *35*, 3438−3440.
(12) Bi, L.; Hu, J.; Jiang, P.; Kim, D. H.; Dionne, G. F.; Kimerling, L. C.; Ross, C. A. On-chip optical isolation in monolithically integrated non-reciprocal optical resonators. *Nat. Photonics* **2011**, *5*, 758−762.

(13) Belotelov, V. I.; Akimov, I. A.; Pohl, M.; Kotov, V. A.; Kasture, S.; Vengurlekar, A. S.; Gopal, A. V.; Yakovelev, D. R.; Zvezdin, A. K.; Bayer, M. Enhanced magneto-optical effects in magnetoplasmonic crystals. *Nat. Nanotechnol.* **2011**, *6*, 370−376.
(14) Chin, J. Y.; Steinle, T.; Wehlus, T.; Dregely, D.; Weiss, T.; Belotelov, V. I.; Stritzker, B.; Giessen, H. Nonreciprocal plasmonics enables giant enhancement of thin-film Faraday rotation. *Nat. Commun.* **2013**, *4*, 1559.
(15) Davoyan, A. R.; Engheta, N. Nonreciprocal rotating power flow within plasmonic nanostructures. *Phys. Rev. Lett.* **2013**, *111*, 047401.
(16) Shadrivov, I. V.; Fedotov, V. A.; Powell, D. A.; Kivshar, Y. S.; Zheludev, N. I. Electromagnetic wave analogue of an electronic diode. *New J. Phys.* **2011**, *13*, 033025.
(17) Soljačić, M.; Luo, C.; Joannopoulos, J. D.; Fan, S. Nonlinear photonic crystal microdevices for optical integration. *Opt. Lett.* **2003**, *28*, 637.
(18) Fan, L.; Wang, J.; Varghese, L. T.; Shen, H.; Niu, B.; Xuan, Y.; Weiner, A. M.; Qi, M. An all-silicon passive optical diode. *Science* **2012**, *335*, 447−50.
(19) Ramezani, H.; Kottos, T.; El-Ganainy, R.; Christodoulides, D. N. Unidirectional nonlinear PT-symmetric optical structures. *Phys. Rev. A* **2010**, *82*, 043803.
(20) Gallo, K.; Assanto, G.; Parameswaran, K. R.; Fejer, M. M. All-optical diode in a periodically poled lithium niobate waveguide. *Appl. Phys. Lett.* **2001**, *79*, 314.
(21) Lira, H.; Yu, Z.; Fan, S.; Lipson, M. Electrically driven nonreciprocity induced by interband photonic transition on a silicon chip. *Phys. Rev. Lett.* **2012**, *109*, 033901.
(22) Fang, K.; Yu, Z.; Fan, S. Photonic Aharonov-Bohm effect based on dynamic modulation. *Phys. Rev. Lett.* **2012**, *108*, 153901.
(23) Kamal, A.; Clarke, J.; Devoret, M. H. Noiseless non-reciprocity in a parametric active device. *Nat. Phys.* **2011**, *7*, 311−315.
(24) Wang, D.-W.; Zhou, H.-T.; Guo, M.-J.; Zhang, J.-X.; Evers, J.; Zhu, S.-Y. Optical diode made from a moving photonic crystal. *Phys. Rev. Lett.* **2013**, *110*, 093901.
(25) Kang, M. S.; Butsch, A.; Russell, P.; St, J. Reconfigurable light-driven opto-acoustic isolators in photonic crystal fibre. *Nat. Photonics* **2011**, *5*, 549−553.
(26) Weis, S.; Riviere, R.; Deleglise, S.; Gavartin, E.; Arcizet, O.; Schliesser, A.; Kippenberg, T. J. Optomechanically induced transparency. *Science* **2010**, *330*, 1520−1523.
(27) Hafezi, M.; Rabl, P. Optomechanically induced non-reciprocity in microring resonators. *Opt. Express* **2012**, *20*, 7672−7684.
(28) Kodera, T.; Sounas, D. L.; Caloz, C. Artificial Faraday rotation using a ring metamaterial structure without static magnetic field. *Appl. Phys. Lett.* **2011**, *99*, 03114.
(29) Wang, Z.; Wang, Z.; Wang, J.; Zhang, B.; Huangfu, J.; Joannopoulos, J. D.; Soljacic, M.; Ran, L. Gyrotropic response in the absence of a bias field. *Proc. Natl. Acad. Sci.* **2012**, *109*, 13194−13197.
(30) Sounas, D. L.; Caloz, C.; Alù, A. Giant non-reciprocity at the subwavelength scale using angular momentum-biased metamaterials. *Nat. Commun.* **2013**, *4*, 2407.
(31) Little, B. E.; et al. Micro-ring resonator channel dropping filters. *J. Lightwave Technol.* **1995**, *2*, 998−1005.
(32) Xu, Q.; Schmidt, B.; Pradhan, S.; Lipson, M. Micrometer-scale silicon electro-optic modulator. *Nature* **2005**, *435*, 325−327.
(33) Xu, Q.; Manipatruni, S.; Schmidt, B.; Shakya, J.; Lispon, M. 12.5 Gbits/s carrier-injection-based silicon micro-ring silicon modulators. *Opt. Express* **2007**, *15*, 430−436.
(34) Niehusmann, J.; et al. Ultrahigh-quality-factor silicon-on-insulator microring resonator. *Opt. Lett.* **2004**, *29*, 2861−2863.

■ NOTE ADDED AFTER ASAP PUBLICATION

This paper was published ASAP on February 13, 2014, with an error in equation 5 and one minor text error on page 4. The corrected version was reposted on February 18, 2014.